An accurate position measurement approach for a single particle in a channel using electrical impedance spectroscopy

An accurate position measurement approach for a single particle in a channel using Electrical Impedance Spectroscopy

*Lu Yang[1], Hongtao Wu[1], Kai Liu[1]**, Bai Chen[1], Jiabin Jia[2], Jianping Li[3], Jiafeng Yao[1]**

1. *College of Mechanical & Electrical Engineering, Nanjing University of Aeronautics, & Astronautics, Nanjing 210016, China*
2. *Agile Tomography Group, Institute for Digital Communications, School of Engineering, The University of Edinburgh, Edinburgh EH9 3JL, U.K.*
3. *College of Engineering, Zhejiang Normal University, Jinhua 321004, China*

Email: yanglu8823@163.com (Lu Yang); mehtwu@126.com (Hongtao Wu); liukai@nuaa.edu.cn(Kai Liu); chenbye@126.com(Bai Chen) ; jiabin.jia@ed.ac.uk (Jiabin Jia); lijp@zjnu.cn (Jianping Li);jiaf.yao@nuaa.edu.cn(Jiafeng Yao)

Corresponding author: Jiafeng Yao; Kai Liu

0 Abstract

A novel position measurement approach for a single particle in a channel using Electrical Impedance Spectroscopy (EIS) only with two pairs of electrodes is proposed. The proposed approach is label-free, non-invasive and is very accurate in measurement domain by using machine learning method. Relationship between the single particle's position and the measured impedances is described by a set of nonlinear equations showing excellent fitting performance with R-square reaching 0.9999. Finding accurate analytical solution of the particle's position is the inverse problem, it is tackled by a well-trained Support Vector Regression (SVR) model with the help of multi-frequency EIS. The proposed approach is evaluated by simulation models with a single particle in 100 different positions. The results show that the approach performs an outstanding position measurement accuracy to reach 99.25%. Comparing with EIT, it has more simple structure, less measurement time and more accurate measurement results.

Keywords: Electrical Impedance Spectroscopy (EIS); multi-frequency measurement; particle position measurement; inverse problem; machine learning

List of symbols

E	Electric field	ω	angular frequency	f	frequency
u	potential	I_l	current of the element of the electrode boundaries	Z_f	impedance at frequency f
σ	conductivity	s	area of the electrode	(x, y)	particle position in Cartesian coordinate system
ε	dielectric constant	Z	impedance	(r, θ)	particle position in Polar coordinates system

1 Introduction

Position tracking of a single particle in the cross section of a channel is always used to analyze its motion properties, study its physical characteristics, provide some feedbacks to control system and many other usages. At present, position estimation of the single particle in fluids is a research hotspot. Optical measurement technology is usually used for position tracking, however, it is hard to measure a single particle flowing in a channel with low transparency. In addition, other

non-contact measuring methods like ultrasonic technology are also not suitable for position tracking of the particle. In recent years, electrical impedance technology has been widely used for particle measurement due to its label-free, non-invasive and low-cost properties [1-3]. Electrical impedance technology is very simple and has wider application scenarios, especially for real-time imaging and long-time monitoring[2, 4, 5]. It is a promising technology to estimate the position of a single particle in fluids.

Electrical Impedance Tomography (EIT), a kind of impedance technology, is widely used for position measurement. It is aiming at reconstruction the distribution of conductivity or conductivity change in the measurement field [6]. For a single particle, position is measured through the reconstruction image. However, contact impedance has a severe effect on EIT sensors as well as the measurement accuracy especially in low frequency [7]. To eliminate contact impedance effect, differential algorithm is used for image reconstruction of EIT [8]. And many efforts have been devoted to solve the inverse problem of EIT by different kinds of differential algorithms, such as Tikhonov Regularization[9], Landweber[10], Newton-Raphson algorithm[11] and many other regularization strategies[12, 13]. While these algorithms are traditional methods with relatively lower reconstruction accuracy due to insufficient measurement information. In addition, some numerically more accurate solutions are used to estimate the location of the target. [3] presents an analytical solution to estimate accurate position of the gas core in two-phase annular flow through a circular pipe using electrical resistance tomography. While the method only performs well when the gas core is close to the centre of the pipe. With the development of artificial intelligence, deep learning methods are used to solve the inverse problem of EIT aiming at getting a better reconstruction image quality. For instance, a conditional generative adversarial network (CGAN) is proposed for image reconstruction and makes the reconstruction images more stable and trustable, moreover, it effectively improves the quality of reconstruction image[14].To improve the generalization ability of deep learning framework, a dominant-current convolutional neural network (CNN)-based inversion method is proposed for image reconstruction of the target with triangular, rectangular, or lung shapes, where the CNN-based method uses only random circle or ellipse training data [15]. Although deep learning scheme has improved the reconstruction image quality and target location accuracy to some extent, it also performs relatively poorer when the target is small. In general, there are some challenges on accurate position measurement of a single particle using EIT.

Electrical Impedance Spectroscopy (EIS) is another kind of electrical impedance technology and it is very sensitive to position. EIS measures the impedance spectroscopy of materials under a set of alternating excitations with continuous frequency[16]. It is widely used for measurement and analysis of materials with dielectric properties such as permittivity and conductivity[17, 18], especially for long time monitoring [19, 20].Comparing with EIT, it has the potential to estimate the single particle's location more accurately with the help of multi-frequency measurement information. Usually, EIS measures particles in solution, suspicion or colloid with uniform distribution, and measurement results reflect the physical or biological properties of particles[21] [22]. For a single particle, EIS measurement results vary with the particle's location in solution, suspicion or colloid. During measuring process, the cell is required to be fixed into the center between the two electrodes[1]. Generally, soft physical field measurement technology EIS has the potential to get more accurate single particle's position.

Different from EIT working under a certain low frequency with a set of electrodes, EIS measurement is conducted only by a pair of electrodes under a succession of frequency through sweeping. EIS is also a kind of soft field measurement technology, it measures dielectric characteristics of particle. The impedance measurements also reflect the changes in position of the single object in the measurement field. In some cases, multi-frequency EIS is used to measure the properties of a single yeast cell in the trap by a newly designed microfluidic device, as well as measure the changes in position or motion of the single yeast cell[23]. On the other hand, EIS is capable to measure particle's position even movement with microfluidic device like a 3-D integrated microchannel-electrode system[24], and is hoped to do some feedback for single object's position control such as cell manipulation[25]. In consideration of the rich application prospects, EIS position measuring approach of single particle detection is worthy of further studying.

In this paper, an accurate position measurement approach for a single particle in a channel using EIS only with two pairs of electrodes is proposed. The proposed approach takes advantages of multi-frequency merits and uses machine learning methods to tackle inverse problem of position measurement. Firstly, in Section 2, relationship between the position of a single particle in solution and its impedance distribution is studied by simulation. Secondly, Support Vector Regression(SVR) model with multi-frequency features is utilized to calculate the precise position, the proposed approach is illustrated in details in Section 3. Thirdly, in Section 4, the proposed approach is evaluated by a set of simulation models, in addition, measurement performance is compared with EIT. Based on the evaluation and comparison results, the proposed approach is further discussed. Finally, in Section 5, conclusions are made and future research proposals are presented.

2 Numerical simulation

In this section, numerical simulation methods are used to get the relationship between the position of a single particle in the measurement domain and its impedance spectroscopy. Alternating current excitation mode are used for simulation, and simulations are according to Equation (1)-(3) [26]. Equation (3) is used for elements near the electrodes' boundaries. Numerical simulation is conducted by a finite element simulation software. The appendix part describes the implementation in simulation software in details.

$$E(x,y) = -\nabla u(x,y) \tag{1}$$

$$\nabla \cdot [(\sigma + j\omega\varepsilon)\nabla u(x,y)] = 0 \tag{2}$$

$$\int (\sigma_l + j\omega\varepsilon_l)\frac{\partial u_l}{\partial n} ds = I_l \tag{3}$$

Where $E(x,y)$ is the electric field at (x,y), $u(x,y)$ is the potential at (x,y), σ is the conductivity at (x,y), ε is the dielectric constant at (x,y), ω is the angular frequency of excitation current, σ_l, ε_l, u_l, I_l are conductivity, dielectric constant, potential, current of the element of the electrode boundaries respectively, $\frac{\partial u_l}{\partial n}$ represents the potential component of normal direction along the electrode, s is the area of the electrode.

2.1 Impedance distribution of a single particle in different positions

To get the impedance distribution of a single particle in different spatial locations, a simulation model is built for qualitative analysis as shown in figure 1. The electrical measurement field is modeled as a circular domain in blue, solution is supposed to put into the measurement domain. Two red electrodes, one is excitation electrode and another is ground electrode, are at two sides of the measurement domain. The two electrodes are also used as the measurement electrodes. The center coordinates of the two electrodes are $(-R,0)$ and $(R,0)$, where R is the radius of measurement domain. The green object is modeled as the measuring particle, where $C(x\_c, y\_c)$ is the center coordinate of the measuring particle. Simulation parameter settings are shown as Table 1.

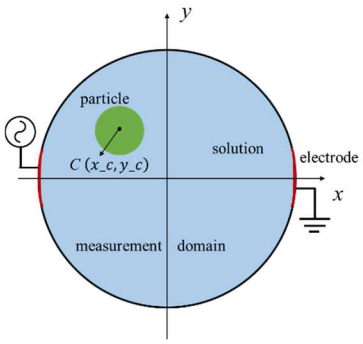

Figure 1. Simulation model with a single particle for impedance measurement

Table 1. Simulation parameter

Attribute	Measurement domain			Particle			Electrode length	Excitation current	Current frequency
	radius	conductivity	relative permittivity	radius	conductivity	relative permittivity			
Value	2.5	0.0001	80	0.5	1.31	60	0.65	0.5	1k~3M
Unit	mm	S/m	1	mm	S/m	1	mm	mA	Hz

To simulate the effect of the green particle's position on measuring impedance, 500 random positions of (x_c, y_c) are generated, where $x\_c \in (-2,2)$, $y\_c \in (-2,2)$. The excitation current frequency range is 1k ~ 3MHz, at each frequency, impedance distribution of the 500 random $C(x\_c, y\_c)$ is generated by simulation. From 1k ~ 3MHz, 6 typical kinds of frequency are chosen to show the impedance distribution. Actually, each frequency shows the same kinds of impedance distribution, the two-dimensional coordinates of the particle and its impedance formed a surface like hyperbolic paraboloid. 6 typical kinds of frequency are 1kHz, 50kHz, 100kHz, 500kHz, 1MHz and 3MHz, their impedance distribution are shown as Figure 2. Figure 2 indicates that distributions are in the same shape and impedance decreases with the increase of frequency.

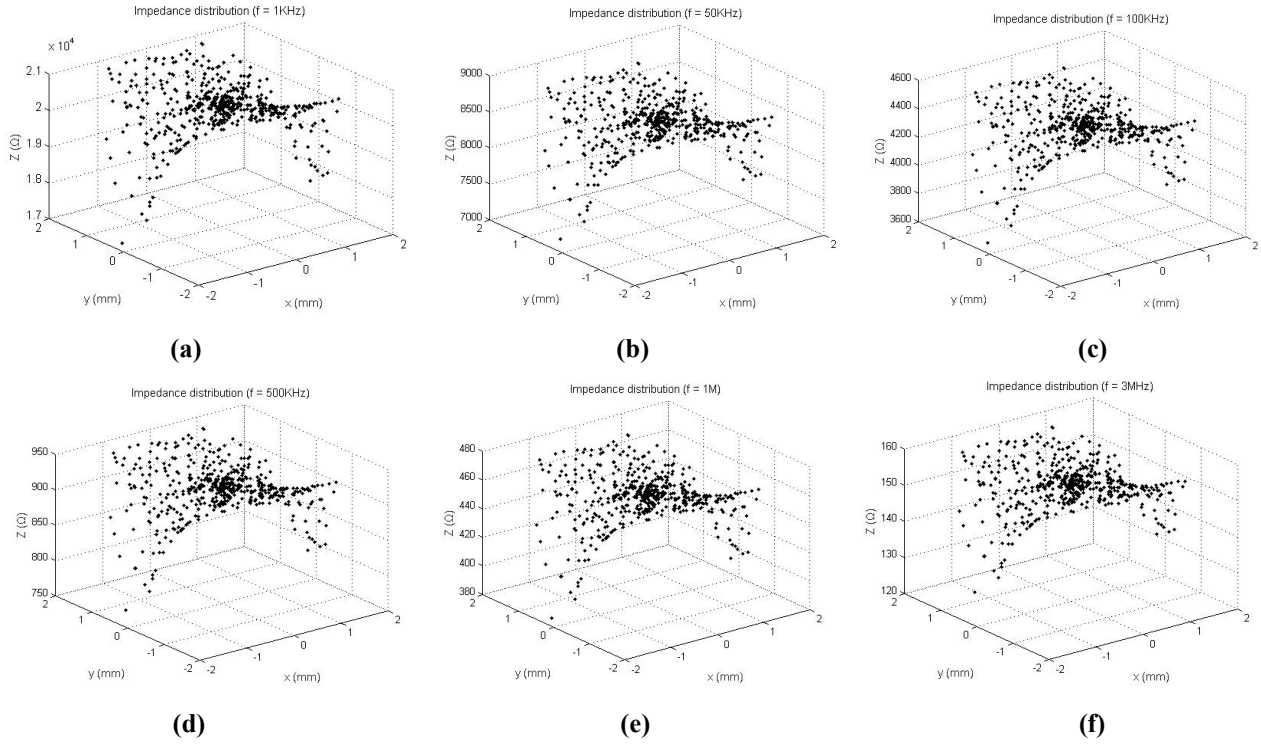

Figure 2. Impedance distribution in different positions. (a) f = 1kHz, (b) f = 50kHz, (c) f = 100kHz, (d) f = 500kHz, (e) f = 1MHz, (f) f = 3MHz

2.2 Surface fitting for impedance distribution

To describe the relationship between particle's position and its impedance in math exactly, firstly, we set $y_c = 0$, x_c is generated randomly range from -2 to 2, and 100 positions are generated for simulation. Then at each frequency, x_c and impedance are fitted quite well by a curve like a parabola going downwards as shown in Figure 3(a) and Equation (4). In the same way, we set $x_c = 0$, y_c is generated randomly range from -2 to 2, and 100 positions are also generated for simulation. Then y_c with the impedance are fitted by a curve like a parabola going upwards as shown in Figure 3(b) and Equation (5). Figure 3 only shows the impedance distribution in x and y directions when the excitation frequency f = 500kHz, actually the impedance distribution in x and y directions follows the same law at each frequency, Equation (4) and Equation (5) with several parameters are also applicable at each frequency. R-square[27] is used to evaluate the goodness

of the fitting results. At each frequency, all R-square reaches 1, means that the fitting equations are generic and reflect the true impedance distribution in *x* and *y* directions.

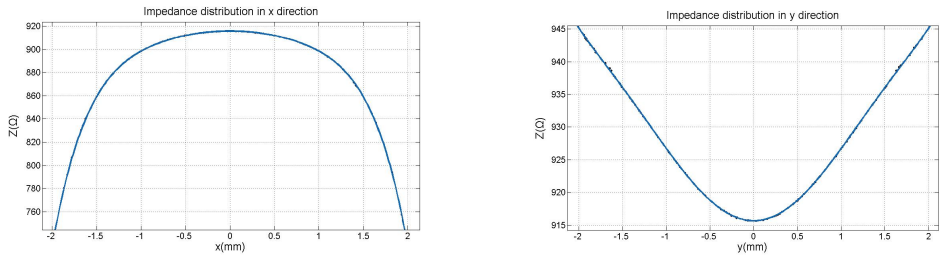

(a) **(b)**

Figure 3. Impedance distribution in *x* and *y* directions. (a) Impedance distribution in *x* direction, where *y* = 0, *x* ranges from -2 to 2, *f* = 500kHz. (b) Impedance distribution in y direction, where *x* = 0, *y* ranges from -2 to 2, *f* = 500kHz.

$$-\frac{x^6}{a1_f{}^2}-\frac{x^4}{b1_f{}^2}-\frac{x^2}{c1_f{}^2}+d1_f=Z_f(x,0) \tag{4}$$

$$\frac{y^6}{a2_f{}^2}-\frac{y^4}{b2_f{}^2}+\frac{y^2}{c2_f{}^2}+d2_f=Z_f(0,y) \tag{5}$$

Where x, y are both coordinates of the center of the particle, Z_f is the impedance when particle is located in $(x,\ y)$ at frequency f. $a1_f$, $b1_f$, $c1_f$, $d1_f$, $a2_f$, $b2_f$, $c2_f$, $d2_f$ are parameters determined by excitation frequency f.

According to Figure 2 and Figure 3, the impedance has symmetrical distribution along *x* and *y* direction. Base on the excitation and measurement mode, the particle position's change along *y* direction is not as large as it in *x* direction. In addition, the surface is similar to a hyperbolic paraboloid which is assumed to predict the relationship between the two-dimensional coordinates of the particle and its impedance distribution. In general, according to Figure 3, Equation (4) and (5), the genetic form of the impedance distribution in a two-dimensional space at each frequency is constructed as Equation (6). In Equation (6), terms of Equation (4) and (5) are combining, three mixed terms where the exponent of *x* is greater than that of *y* are added to get better goodness of the fitting. Actually, the more mixed terms, the better goodness of fitting. More terms mean more parameters. According to excitation and measurement mode, 3 mixed terms are enough. There are 10 parameters in Equation (6), $a1_f$, $b1_f$ and $c1_f$ are parameters of term with x, $a2_f$, $b2_f$ and $c2_f$ are parameters of term with y, $p1_f$, $p2_f$ and $p3_f$ are parameters of the mixed term, d_f is a constant term related to the impedance when particle is located in $(0,\ 0)$ as well as the contact impedance between the electrode and solution. Equation (6) is a generic one to describe the impedance distribution of different positions.

$$-\frac{x^6}{a1_f{}^2}-\frac{x^4}{b1_f{}^2}-\frac{x^2}{c1_f{}^2}+\frac{y^6}{a2_f{}^2}-\frac{y^4}{b2_f{}^2}+\frac{y^2}{c2_f{}^2}+d_f+p1_f x^6y^2+p2_f x^4y^2+p3_f x^2|y|=Z_f(x,y) \tag{6}$$

Where $a1_f$, $b1_f$, $c1_f$, $a2_f$, $b2_f$, $c2_f$, d_f, $p1_f$, $p2_f$, $p3_f$ are parameters determined by excitation frequency f.

The fitting result of impedance distribution at 500kHz using Equation (6) is shown in Figure 4. Table 2 show the fitting parameter $a1_f$, $b1_f$, $c1_f$, $a2_f$, $b2_f$, $c2_f$, d_f, $p1_f$, $p2_f$, $p3_f$ and the fitting index *R-square*, *RMSE* (Root Mean Square Error)[28] at frequency 1kHz, 50kHz, 100kHz, 500kHz, 1MHz, 1.5MHz, 2MHz, 3MHz. Comparing with the measured impedance, *RMSE* at each frequency are very small, *R-square* at each frequency are all reaching 0.9999. It is a good fitting model when *R-square* is very close to 1 and *RMSE* is very small. Actually, each frequency from 1k-3MHz, all the *R-square* reaches 0.9999 showing excellent goodness of the fitting. Equation (6) reflect the impedance distribution in different positions perfectly. Moreover, the form of Equation (6) is generic, it is applicable for many other cases with the same excitation and measurement mode, and is expected to get perfect fitting performance.

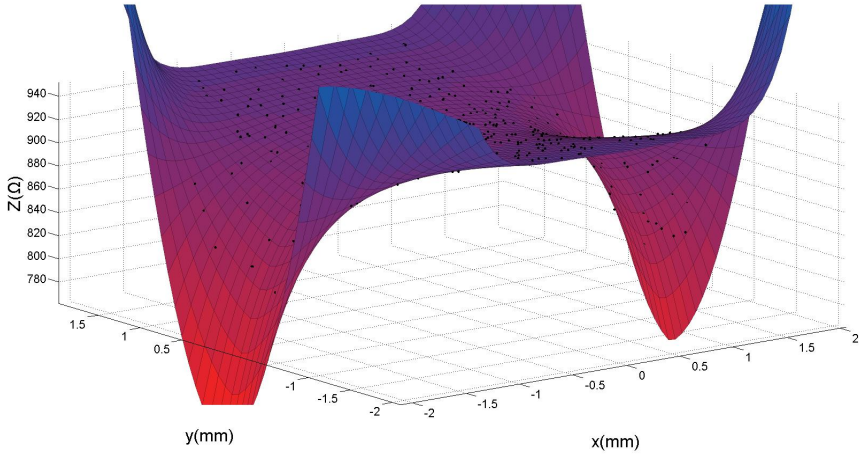

Figure 4. Surface fitting for impedance distribution

Table 2. Fitting parameter at each frequency

Frequency (Hz)	$a1_f$	$b1_f$	$c1_f$	$a2_f$	$b2_f$	$c2_f$	$p1_f$	$p2_f$	$p3_f$	d_f	R-square	RMSE
1k	0.1551	1128	0.05174	0.4889	0.143	0.05879	78.84	-74.74	252.1	20370	0.9999	6.126
50k	0.2404	2484	0.08008	0.7608	0.2223	0.09118	29.5	-31.08	105.1	8488	0.9999	2.792
100k	0.3363	3672	0.112	1.055	0.3099	0.1275	15.07	-15.83	53.67	4339	0.9999	1.427
500k	0.7316	4739	0.2439	2.376	0.6837	0.2781	3.191	-3.414	11.42	915.7	0.9999	0.3032
1M	1.037	2470	0.3455	3.26	0.9564	0.3933	1.584	-1.664	5.64	455.9	0.9999	0.1499
1.5M	1.269	3977	0.4227	3.984	1.17	0.4811	1.058	-1.112	3.768	304.7	0.9999	0.1002
2M	1.465	2594	0.4878	4.614	1.352	0.5553	0.7948	-0.836	2.831	228.8	0.9999	0.0752
3M	1.793	4671	0.5971	5.662	1.656	0.6798	0.5305	-0.559	1.89	152.7	0.9999	0.0502

3 Measurement methodology

3.1 Measurement system calibration

In this section, the proposed approach about single particle position measurement by EIS is introduced in detail. In simulation part, the impedance spatial distribution is described by Equation (6).For a certain particle, suppose that x and y are known, $Z_f(x,y)$ is measured at frequency f, $a1_f$, $b1_f$, $c1_f$, $a2_f$, $b2_f$, $c2_f$, d_f, $p1_f$, $p2_f$, $p3_f$ are parameters needed to be calibrated. However, after the ten parameters are obtained by calibration, (x,y) couldn't be derived through a pair of electrodes cause there are two unknowns. In addition, the impedance distribution is symmetrical along the *x* and *y* axes, solution of the equations is not unique. Consequently, at least two pairs of electrodes and more than one excitation mode are needed to derive the particle's position (x,y).

In measurement system, two pairs of electrodes are installed with a deflection angle α, as shown in Figure 5. In calibration step, electrode pairs (*A, A'*) and (*B, B'*) work separately. Based on $x-y$ and $x'-y'$ coordinate system, ten parameters $a1_f$, $b1_f$, $c1_f$, $a2_f$, $b2_f$, $c2_f$, d_f, $p1_f$, $p2_f$, $p3_f$ could be derived from two equations according to Equation (6) with 5 positions. Relationship between the two plane coordinate system is shown in Equation (7). The calibration results are very important for the next measurement step.

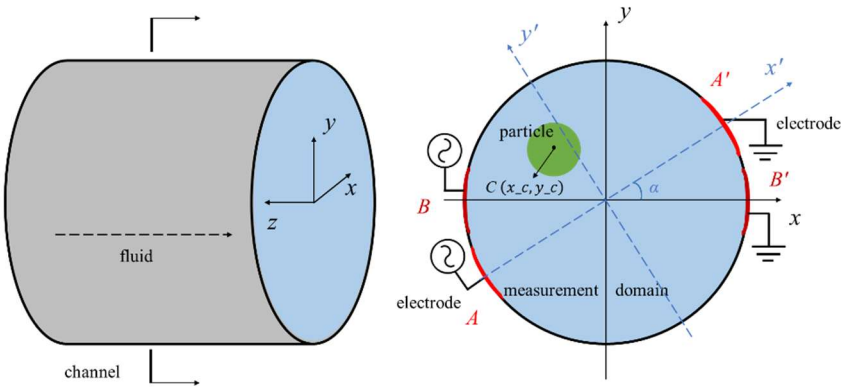

Figure 5. Measurement system with two pairs of electrodes

$$\begin{bmatrix} x' \\ y' \end{bmatrix} = \begin{bmatrix} cos\alpha & sin\alpha \\ -sin\alpha & cos\alpha \end{bmatrix} \begin{bmatrix} x \\ y \end{bmatrix} \tag{7}$$

Where $(x, y), (x', y')$ are the center of the particle in $x - y$ and $x' - y'$ coordinate system, $\alpha (0 < \alpha < \pi/2)$ is the deflection angle of $x' - y'$ coordinate system.

In measurement steps, ten parameters are given by calibration, x, y could be derived from two equations according to Equation (6)

. Due to the impedance distribution is symmetrical along *x* and *y* direction, there are two origin-symmetric solutions of the equations. To tackle the problem, another excitation mode is added. It is introduced in the next measurement section.

3.2 Support Vector Regression (SVR) for position measurement

After calibration, position of the single particle with the same material and same size as calibration used is measured by the proposed approach. At a certain frequency f, $Z_f(x, y)$ and $Z_f{}'(x', y')$ are measured by electrode pairs (*A, A'*) and (*B, B'*) respectively, relationship between (x, y) and (x', y') follows Equation (7), (x, y) is the particle's position to be estimated. Equation (8) shows the details where $a1_f$, $b1_f$, $c1_f$, $a2_f$, $b2_f$, $c2_f$, d_f, $p1_f$, $p2_f$, $p3_f$ are calibrated. Due to the two pairs of electrodes are in the same structure, ten calibration parameters of the two coordinate system are the same.

$$\begin{cases} -\frac{x^6}{{a1_f}^2} - \frac{x^4}{{b1_f}^2} - \frac{x^2}{{c1_f}^2} + \frac{y^6}{{a2_f}^2} - \frac{y^4}{{b2_f}^2} + \frac{y^2}{{c2_f}^2} + d_f + p1_f x^6 y^2 + p2_f x^4 y^2 + p3_f x^2 |y| = Z_f(x, y) \\ -\frac{x'^6}{{a1_f}^2} - \frac{x'^4}{{b1_f}^2} - \frac{x'^2}{{c1_f}^2} + \frac{y'^6}{{a2_f}^2} - \frac{y'^4}{{b2_f}^2} + \frac{y'^2}{{c2_f}^2} + d_f + p1_f x'^6 y'^2 + p2_f x'^4 y'^2 + p3_f x'^2 |y'| = Z_f{}'(x', y') \end{cases} \tag{8}$$

Where (x, y) and (x', y') represent the particle's position in $x - y$ and $x' - y'$ coordinate system respectively, $a1_f$, $b1_f$, $c1_f$, $a2_f$, $b2_f$, $c2_f$, d_f, $p1_f$, $p2_f$, $p3_f$ are given by calibration. $Z_f(x, y)$ and $Z'_f(x', y')$ are impedance measured by two pairs of electrodes respectively.

For the multi-frequency measuring system, EIS is measured by two excitations applied by electrode pairs A and B respectively. The center coordinates of the particle (x, y) and the measured impedance follows Equation(8) at each frequency. The problem is how to calculate (x, y) from Equation (7) and Equation (8). However, it's very hard to obtain the global uniqueness of nonlinear equations like Equation (8). In many cases, the inverse problem[29] is hard. Consequently, inverse problem like nonlinear equations' problems are always converted to optimization problem [30, 31]. Regularization methods are always used for inverse problem[32]. In addition, many efforts have been devoted to the optimization problem, such as Stochastic gradient descent (SGD)[33], Gauss-Newton algorithm[34], Genetic algorithm(GA)[35] and so on. In our application, global optimal solution for Equation (7) and (8) is needed. Taking the advantages of EIS with multi-frequency impedance, machine learning methods are considered to be applicable to get the optimal precise solution by large amounts of training samples with sufficient features obtained from EIS.

Due to the highly nonlinear characteristics of Equation (8), description of particle's center (x, y) and (x', y') in two

Cartesian coordinate system are converted to polar coordinates as described in Equation (9). Then the problem to solve particle's position (x, y) is converted to solve (r, θ) according to Equation (8) and Equation (9). It is possible to get r using impedance features from EIS of the two pairs of electrodes by machine learning methods. Support Vector Regression (SVR) is an excellent machine learning method for regression[36]. SVR with radial basis function as kernel function is utilized to get the global optimal solution of optimization problem to solve Equation(8) and (9). Equation(10) explains the detail of SVR using radial basis function as kernel function.

$$\begin{cases} x = r\cos(\theta) \\ y = r\sin(\theta) \\ x' = r\cos(\theta - \alpha) \\ y' = r\sin(\theta - \alpha) \end{cases} \tag{9}$$

Where r is the distance between particle's center and the origin , θ is the particle center's deflection angle relative to x axis.

$$L(w) = \frac{1}{2}\|w\|^2 + \frac{1}{2}C\sum_{i=1}^{n}(\xi_i^2 + \xi'^2_i)$$

$$K(x, z) = \phi(x) \cdot \phi(z) = \exp(-\frac{\|x - z\|^2}{2\sigma^2})$$

$$f(x) = \ w \cdot \phi(x) + b$$

$$s.t. \quad y_i - f(x_i) \le \epsilon + \xi_i$$

$$f(x_i) - y_i \le \epsilon + \xi'_i$$

$$\epsilon \ge 0, \xi_i \ge 0, \xi'_i \ge 0, i = 1,2, \dots, n \tag{10}$$

Where $L(w), K(x, z), f(x)$ represent the loss function, kernel function, regression function respectively. w, b are the weight and bias of regression function. ϵ, ξ_i and ξ'_i are very tiny positive number. i from 1 to n is the number of training examples. C is the penalty coefficient which is a positive number.

As a matter of convenience, we define the estimated position vector in polar coordinates as $\hat{p} = (\hat{r}, \hat{\theta})$. There are two unknowns r, θ and two equations, so uniqueness of solution could be derived in a quadrant. The equations shows that there is a relationship between the unknown r and the two measured impedances. EIS contains multi-frequency impedance, could be used as the features to feed the SVR model to derive the unknown r. At first, electrical impedance spectroscopy of the two pairs of electrodes are measured, several typical frequencies are selected for measurement, they are described as a vector $F = \{f_1, f_2, f_3, \dots, f_n\}$. For any $f_i \in F$, $a1_{f_i}$, $b1_{f_i}$, $c1_{f_i}$, $a2_{f_i}$, $b2_{f_i}$, $c2_{f_i}$, d_{f_i}, $p1_{f_i}$, $p2_{f_i}$, $p3_{f_i}$ are known from calibration process, $Z_{f_i}(r, \theta)$, $Z_{f_i}(r, \theta - \alpha)$, are obtained from the measured electrical impedance spectroscopy. Secondly, a feature set $\{Z_{f_1}, Z'_{f_1}, Z_{f_2}, Z'_{f_2}, \dots, Z_{f_n}, Z'_{f_n}\}$ at some frequency f from F are used as the input of SVR model, r is the output of SVR. Secondly, a set of samples are generated by forward process of Equation (8) and (9) to train and test SVR model. The samples are divided into five sections randomly, four of them are for training, the rest is for testing. A five-fold cross validation method is used to choose the best SVM model and evaluate the SVR model comprehensively. Thirdly, given a new feature example, polar diameter $\hat{r}$ could be obtained from the trained SVR model. Finally, polar angle $\hat{\theta}$ could be calculated from Equation (8) and (9) with the help of $\hat{r}$. However, there are still two solutions with π difference for θ, another excitation mode is added to solve the problem. Figure 6 and 7 illustrate the measurement process using SVR in detail.

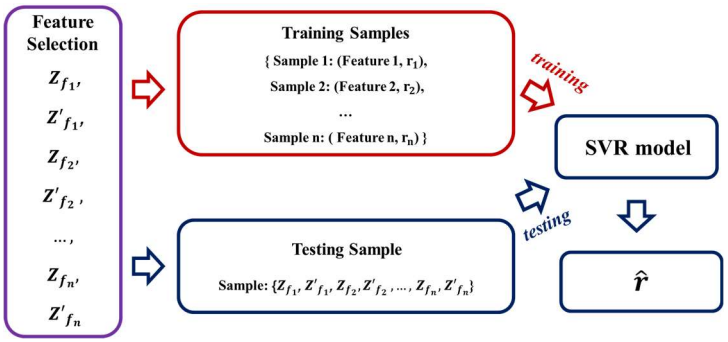

Figure 6. Estimation the polar diameter $\hat{r}$ by a SVR model

After $\hat{r}$ is estimated from the trained SVR model, Z_f and $Z_f{}'$ only vary with θ according to Equation (8) and (9). When Z_f and $Z_f{}'$ are given, there are two solutions for θ. The phase difference of the two solutions is π. As shown in Figure 7, the measured impedance varying with angle forms a curve like a sine wave. When Z_f and $Z_f{}'$ are given, $\theta 1$ and $\theta 2$ are two solutions of Equation (8). To judge which one is the real solution, adjacent excitation mode is added to assist measuring. Electrode A and B, electrode A' and B' are regarded as a pair of electrode to do adjacent excitation respectively. If particle is closer to the electrode pair (A ,B) than (A', B'), the measured impedance of (A ,B) is smaller than (A', B') in case of the particle has higher electrical conductivity. Finally, θ could be estimated.

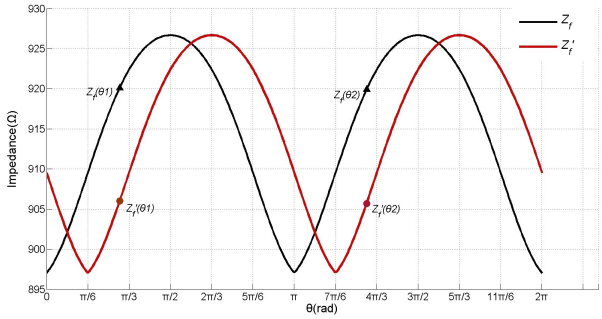

Figure 7. Relationship between polar angle θ and the measured impedance Z_f, $Z_f{}'$

3.3 Measurement workflow

The main steps of our workflow for single particle's position measurement using EIS is given as follows:

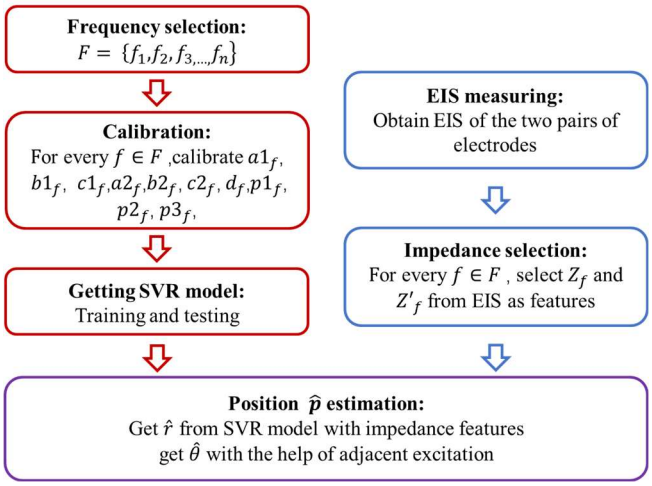

Figure 8. Measurement workflow

(1) **Frequency selection:** several typical frequencies are selected for measurement which are described as a vector $F = \{f_1, f_2, f_{3,\ldots}, f_n\}$.

(2) **Calibration:** for every $f \in F$, ten parameters $a1_f$, $b1_f$, $c1_f$, $a2_f$, $b2_f$, $c2_f$, d_f, $p1_f$, $p2_f$, $p3_f$ are calibrated according to Equation (6) with 5 positions.

(3) **Getting SVR model:** the estimated particle position vector in polar coordinates is supposed as $\hat{p} = (\hat{r}, \hat{\theta})$, a feature set $\{Z_{f_1}, Z'_{f_1}, Z_{f_2}, Z'_{f_2}, \ldots, Z_{f_n}, Z'_{f_n}\}$ are selected as the input of SVR model, r is the output of SVR. Then a set of samples are generated by forward process of Equation (8) and (9) to train and test SVR model.

(4) **EIS measuring and impedance selection:** Obtain EIS of the two pairs of electrodes: (A, A') and (B, B'), for every $f \in F$, select Z_f and Z'_f from EIS as features to estimate r using the trained SVR model.

(5) **Position $\hat{p}$ estimation:** Get $\hat{r}$ from SVR model with impedance features, using adjacent excitation to judge the particle's quadrant, finally get $\hat{\theta}$ by Equation (8).

4 Methodology evaluation

In this section, the proposed measurement approach is evaluated comprehensively. To demonstrate its advantages, measurement performance is compared with EIT. Simulation models with the single particle in 100 different positions are generated for evaluation and comparison. Based on the evaluation and comparison results, the proposed approach is further discussed.

4.1 Measurement performance evaluation

As the measurement workflow mentioned in section 3, firstly, a set of frequencies with eight typical frequencies $F = \{1k, 50k, 100k, 500k, 1M, 1.5M, 2M, 3M\}$ are chosen for calibration and measurement. Secondly, for every $f \in F$, ten parameters $a1_f$, $b1_f$, $c1_f$, $a2_f$, $b2_f$, $c2_f$, d_f, $p1_f$, $p2_f$, $p3_f$ are calibrated as Table 2. Thirdly, 16 features $\{Z_{1k}, Z'_{1k}, Z_{50k}, Z'_{50k}, \ldots, Z_{3M}, Z'_{3M}\}$ are assembled as the inputs of SVR model. Training and testing process of the SVR model are shown in Figure 6. Due to highly nonlinear properties, large amounts of samples are needed for training. 25000 samples which are generated from equation (8) and (9) are divided into 5 sections. In each experiment, one section is selected for testing, and others are for training, so there are five experiments in total. *R-square* and *RMSE* are utilized to evaluate the regression performance of predicting r, the training and testing results of SVM model is shown in Table 3.Average *R-square* of training and testing is 0.9982 and 0.9971 respectively, very close to 1.Moreover, Average *MAE*(Mean Absolute Error)[28] is 0.0121 and 0.0139 for training and testing, which is very small. That means the SVR model is trained very well to get precise r. Experiment 2's trained model is selected as the final SVR model due to its better testing performance.

Table 3. Training and testing for SVR

Indicator	Training						Testing					
	# 1	# 2	# 3	# 4	# 5	Average	# 1	# 2	# 3	# 4	# 5	Average
R-square	0.9982	0.9982	0.9982	0.9982	0.9982	0.9982	0.9971	0.9972	0.9970	0.9975	0.9966	0.9971
MAE (mm)	0.0121	0.0122	0.0122	0.0120	0.0121	0.0121	0.0139	0.0136	0.0136	0.0138	0.0147	0.0139

After SVR model is trained well, EIS which are measured from the two pairs of electrodes are ready to estimate the single particle's position. As shown in Figure 8, at a certain frequency, $\hat{\theta}$ is easily derived from Equation (8) in a quadrant after getting $\hat{r}$ from SVR model. Adjacent excitation is used to judge which quadrant the particle belongs to. Measurement results of the single particle in 100 positions are shown in Table 4. *Accuracy* is the ratio of *MAE* to the full-scale of measurement domain. In polar coordinate system, *MAE* of polar radius and polar angle are 0.0263mm and 0.0298 rad respectively. In Cartesian coordinate system, *MAE* is 0.0302mm in *x* direction, and it is 0.0271mm in *y* direction. The measurement accuracy is as high as 99.25%. It proves that the proposed approach makes excellent

performance for a single particle position measurement.

Table 4. Measurement performance

Indicator	Polar coordinates system		Cartesian coordinate system	
	r	θ	x	y
MAE	0.0263 mm	0.0298 rad	0.0302 mm	0.0271mm
Accuracy	98.69%	99.53%	99.25%	99.32%

4.2 Measurement performance comparison

To demonstrate the proposed approach's advantages, position measurement performance comparison is conducted between our method and EIT. An 8-electrode EIT sensor is used for imaging. Position of the single particle is calculated according to EIT reconstruction images by image processing methods. Simulation models with the single particle in 100 different positions are available for comparison. *MAE_X, MAE_Y, Electrode, Excitation* and *Measurement* are five indicators to illustrate comparison results. *MAE_X* is the Mean Absolute Error in *x* direction, *MAE_Y* is the Mean Absolute Error in *y* direction, *Electrode* indicates the number of electrodes, *Excitation* indicates the excitation times, *Measurement* is the measuring times. As shown in Table 5, the proposed approach gets a better measuring performance than EIT using only 4 electrodes with 4 excitations and 4 measurements. It has more simple structure, less measurement time and more accurate measurement results than EIT. It is predictable that the proposed approach would present much superiority in measuring accuracy when the particle is in small size.

Table 5. Measurement performance comparison

Indicator	MAE_X	MAE_Y	Electrode	Excitation	Measurement
EIT	0.0545 mm	0.0428 mm	8	8	20
The proposed approach	0.0302 mm	0.0271 mm	4	4	4

4.3 Discussion

Some important points should be noted in application. Firstly, electrical field is a soft field, the solution in the measurement domain is not completely isotropic, so there is a slight difference in each measurement. When using the proposed approach, the greater the difference in conductivity between the solution and the particle, the better. Secondly, a set of frequencies are selected for measurement, low and high frequencies are needed to be avoid. Because when measurement is conducted at low frequency, the impedance may be too large to be out of the impedance analyzer's range, the measurement results are untrusted. Similarly, at high frequency, the impedance change caused by position is very small and may not be measured. Several frequencies are enough for measurement. Thirdly, in real application, data acquisition rate should match with the velocity of flow, the dynamic effect of the particle should be considered. Moreover, higher machining accuracy of electrodes is required. Due to the existence of measurement error of the system, measuring accuracy is lower than simulation.

The highlight of this paper is describing the relationship between the single particle's position and the measured impedances by a set of nonlinear equations and finding accurate analytical solution by machine methods. Getting the impedances from position is forward problem, while calculating the precise position of particle according to the measured electrical impedances is inverse problem. The inverse problem is always hard, while it is tackled by trained a SVR model in this paper. The proposed approach could be generalized to non-circle shape inclusions, such as polygon, ellipse and so on. Different from circle targets, the direction of non-circle inclusion has an effect on the measured impedances. Thus relationship between the direction of non-circle targets and the measured impedances should be studied further. Machine learning methods are also suitable to find the accurate analytical solution of the non-circle target's position.

5 Conclusions

In this paper, a novel position measurement approach for a single particle in a channel using EIS with two pairs of electrodes is proposed. In our work, relationship between the single particle's position and the measured impedances is described by a set of nonlinear equations. Machine learning methods is innovatively used to tackle the inverse problem to find accurate analytical solution of the single particle's position. The proposed approach makes excellent performance for position estimation of a single particle, the measurement accuracy is as high as 99.25%. Comparing with EIT, *MAE* in x direction is improved from 0.0545 mm to 0.0302mm, and *MAE* in y direction is improved from 0.0428 mm to 0.0271 mm.

In general, the proposed approach has achieved good performance in position estimation of a single particle. For future research, more works could be done to improve measurement performance. Two aspects of future study are discussed as follows: (1) A trained SVR model is introduced to tackle the inverse problem of position tracking in this paper. However, the machine learning model, feature selection and training strategy have great effects on measurement accuracy. Future study on more appropriate models, features and training strategy are needed to improve measurement accuracy. (2) The proposed approach could be generalized to non-circle shape inclusions, such as polygon, ellipse and so on. The generalization methods are required to be further studied. Direction of non-circle inclusion has an effect on the measured impedances. Thus relationship between the direction of non-circle targets and the measured impedances should be studied further.

6 Acknowledgement

This work was supported by the National Natural Science Foundation of China [grant number 62071224, 51706098]; the Natural Science Foundation of Jiangsu Province [grant number BK20170792].

7 Appendix

Numerical simulation is conducted by COMSOL Multiphysics. Programs in Matlab language about simulation implementation is attached as the supplementary material. In addition, 25000 samples with different excitation frequencies and particle positions are used for training and testing. The detailed assignment of the samples is attached as the supplementary material.

8 References

[1] Y. Xu, X. Xie, Y. Duan, L. Wang, J. Cheng, A review of impedance measurements of whole cells, Biosensors & Bioelectronics, 77 (2016) 824-836.

[2] H. Chen, J. Yao, L. Yang, K. Liu, S. Wang, B. Chen, J. Li, M. Takei, Development of a portable Electrical Impedance Tomography device for online thrombus detection in extracorporeal-circulation equipment, IEEE Sensors Journal (2020) (In press).

[3] R. Wang, B.A. Lee, J.S. Lee, K.Y. Kim, S. Kim, Analytical estimation of liquid film thickness in two-phase annular flow using electrical resistance measurement, Applied Mathematical Modelling, 36 (2012) 2833-2840.

[4] Y. Zhou, X. Li, A real-time EIT imaging system based on the Split Augmented Lagrangian Shrinkage Algorithm, Measurement, 110 (2017) 27-42.

[5] D.N. Huu, D. Kikuchi, M. Takei, A. Sapkota, Monitoring of thrombus formation in mock extracorporeal circulation system using electrical impedance spectroscopy, 2016 International Conference on Biomedical Engineering (BME-HUST), 2016.

[6] B.H. Brown, Electrical impedance tomography (EIT): a review, J. Med. Eng. Technol. , 27 (2003) 97-108.

[7] X. Liu, J. Yao, T. Zhao, H. Obara, Y. Cui, M. Takei, Image reconstruction under contact impedance effect in micro Electrical Impedance Tomography sensors, IEEE Trans. Biomed. Circuits Syst. , 12 (2018) 623-631.

[8] L. Ying, L. Rao, R. He, G. Xu, Image reconstruction of EIT using differential evolution algorithm, International Conference of the IEEE Engineering in Medicine & Biology Society, 2003, pp. 1011-1014.

[9] S. Oh, T. Tang, R.J. Sadleir, Quantitative analysis of shape change in Electrical Impedance Tomography (EIT), International Conference Electrical Bioimpedance, 2007, pp. 424-427.

[10] W. Yang, L. Peng, Image reconstruction algorithms for electrical capacitance tomography, Meas. Sci. Technol. , 14 (2002) R1-R13.

[11] H.-C. Kim, C.-J. Boo, M.-J. Kang, Image reconstruction using Genetic Algorithm in Electrical Impedance Tomography, Springer Berlin Heidelberg, Berlin, Heidelberg, 2006, pp. 938-945.

[12] S.I. Kang, A.K. Khambampati, B.S. Kim, K.Y. Kim, EIT image reconstruction for two-phase flow monitoring using a sub-domain based regularization method, Flow Measurement & Instrumentation, 53 (2017) 28-38.

[13] T.K. Bera, S.K. Biswas, K. Rajan, J. Nagaraju, Projection Error Propagation-based Regularization (PEPR) method for resistivity reconstruction in Electrical Impedance Tomography (EIT), Measurement, 49 (2014) 329-350.

[14] Y. Chen, K. Li, Y. Han, Electrical resistance tomography with conditional generative adversarial networks, Meas. Sci. Technol. , 31 (2020) 055401.

[15] Z. Wei, D. Liu, X. Chen, Dominant-Current deep learning scheme for Electrical Impedance Tomography, IEEE Trans. Biomed. Eng. , 66 (2019) 1546-2555.

[16] Z. Jiang, J. Yao, L. Wang, H. Wu, J. Huang, T. Zhao, M. Takei, Development of a portable Electrochemical Impedance Spectroscopy system for bio-detection, IEEE Sens. J. , 19 (2019) 5979-5987.

[17] K. Asami, T. Yonezawa, Dielectric behavior of wild-type yeast and vacuole-deficient mutant over a frequency range of 10 kHz to 10 GHz, Biophys. J . , 71 (1996) 2192-2200.

[18] T. Sun, N.G. Green, H. Morgan, Analytical and numerical modeling methods for impedance analysis of single cells on-chip, Nano, 03 (2008) 55-63.

[19] K. Asami, T. Yonezawa, Dielectric analysis of yeast-cell growth, Biochimica Et Biophysica Acta-General Subjects, 1245 (1995) 99-105.

[20] B. Sanchez, A. Guasch, P. Bogonez, C. Galvez, V. Puig, C. Prat, C.E. Semino, A. Bayesgenis, R. Bragos, Towards on line monitoring the evolution of the myocardium infarction scar with an implantable electrical impedance spectrum monitoring system, Conf Proc IEEE Eng Med Biol Soc, 2012 (2012) 3223-3226.

[21] K. Asami, Low-frequency dielectric dispersion of bacterial cell suspensions, Colloids Surf B Biointerfaces, 119 (2014) 1-5.

[22] K. Asami, K. Sekine, Dielectric modelling of cell division for budding and fission yeast, Journal of Physics D-Applied Physics, 40 (2007) 1128-1133.

[23] Z. Zhu, O. Frey, F. Franke, N. HaandbaeK, A. Hierlemann, Real-time monitoring of immobilized single yeast cells through multifrequency electrical impedance spectroscopy, Analytical & Bioanalytical Chemistry, 406 (2014) 7015-7025.

[24] J. Yao, H. Obara, A. Sapkota, M. Takei, Development of three-dimensional integrated microchannel-electrode system to understand the particles' movement with electrokinetics, Biomicrofluidics, 10 (2016) 87-105.

[25] Voldman, Joel, Electrical forces for microscale cell manipulation, Annual Review of Biomedical Engineering, 8 (2006) 425-454.

[26] L.K. Taghizadeh, Ahmad; Stadlbauer, Benjamin; Weninger, Wolfgang J.; Kaniusas, Eugenijus; Heitzinger, Clemens, Bayesian inversion for electrical-impedance tomography in medical imaging using the nonlinear Poisson—Boltzmann equation, Computer Methods in Applied Mechanics and Engineering, 365 (2020) 112959.

[27] W. Yun, On efficiency properties of an R-square coefficient based on final prediction error, Statistics &

Probability Letters, 83 (2013) 2276-2281.
[28] C. Willmott, K. Matsuura, Advantages of the mean absolute error (MAE) over the root mean square error (RMSE) in assessing average model performance, Climate Research, 30 (2005) 79.
[29] A. Tarantola, Inverse problem theory and methods for model parameter estimation, Society for Industrial & Applied Mathematics Philadelphia Pa, (2005) xii,342.
[30] W. Song, Y. Wang, H.X. Li, Z. Cai, Locating multiple optimal solutions of nonlinear equation systems based on multiobjective optimization, IEEE Trans. Evol. Comput. , 19 (2015) 414-431.
[31] S. Sadiqbatcha, S. Jafarzadeh, Y. Ampatzidis, Particle swarm optimization for solving a class of type-1 and type-2 fuzzy nonlinear equations, Soft Computing, 2018, pp. 103-110.
[32] G. Peyre, S. Bougleux, L.D. Cohen, Non-local regularization of inverse problems, European Conference on Computer Vision, 2008, pp. 57-68.
[33] Y. Ermoliev, Facility location problem. Numerical techniques for stochastic optimization, Springer, (1988).
[34] M.R. Osborne, Separable least squares, variable projection, and the gauss-newton algorithm, ETNA. Electronic Transactions on Numerical Analysis [electronic only], 28 (2007) 1-15.
[35] D.E. Goldberg, D.M. Goldberg, D.E. Goldberg, D. Goldberg, E.D. Goldberg, E. Goldberg, E. Goldberg, D. Goldberg, T.B.L. Goldberg, A. De De, Genetic algorithm is search optimization and machine learning, (1989).
[36] A.J. Smola, B. Scholkopf, A tutorial on support vector regression, Statistics and Computing, 14 (2004) 199-222.